33

A Single-compartment Model of Calcium Dynamics in Nerve Terminals and Dendrites

FRITJOF HELMCHEN AND DAVID W. TANK

INTRODUCTION

In this chapter, we describe a single-compartment model of calcium dynamics that has been applied to fluorescence measurements of calcium transients in neurons. It has been particularly useful in describing the buildup and decay of the intracellular free calcium concentration ($[Ca^{++}]_i$) produced by sodium action potentials in nerve terminals and dendrites (Regehr and Tank 1994). Rapid (<1 msec) and local (<0.1 μm) actions of Ca^{++} near its entry site, such as the triggering of neurotransmitter release by calcium microdomains (see Chapter 38), are not addressed by this approach. Rather, the model describes the dynamics of longer lasting (typically >10 msec) and more spatially homogeneous $[Ca^{++}]_i$ elevations—sometimes referred to as "residual free calcium"—that are commonly measured in dendrites and nerve terminals with high-affinity calcium indicators such as Fura-2 and Calcium Green-1.

We first describe the model under the conditions of fast, nonsaturating buffers for which analytical expressions for the amplitude and the time constants of $[Ca^{++}]_i$ changes can be explicitly derived. We present examples of how this model has been applied to experimental data to obtain quantitative information about Ca^{++} influx, buffering, and clearance. We then illustrate several changes that occur when saturation or kinetic effects become significant. Finally, we discuss how the changes in calcium dynamics that are explained by the model have been exploited for measuring properties of calcium-driven reactions, such as those regulating short-term synaptic enhancement, vesicle recycling, and adaptation.

THE SINGLE-COMPARTMENT MODEL

The underlying assumption is that Ca^{++} gradients and diffusion can be neglected on the time scale of interest, making it possible to treat the cytosolic volume as a single,

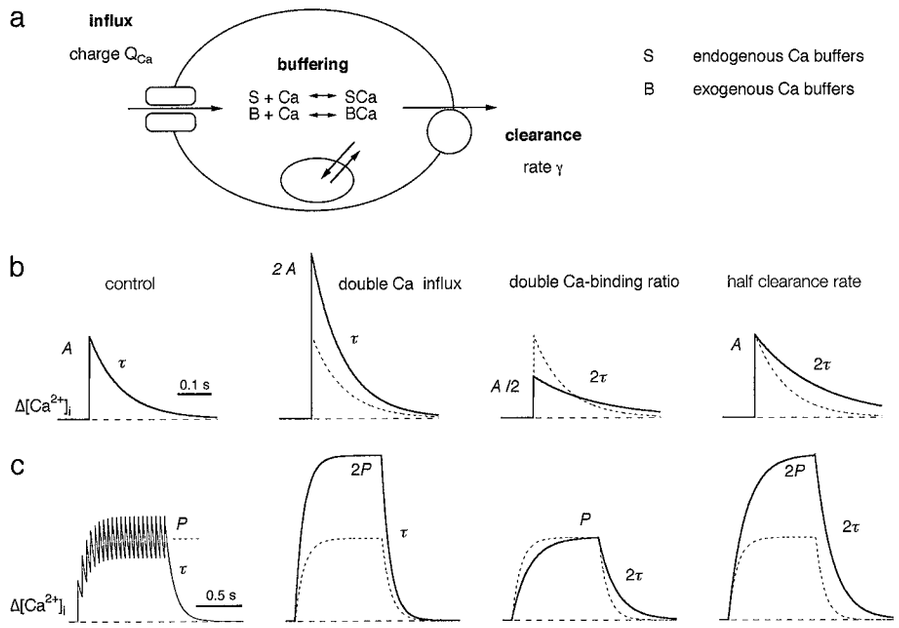

Figure 33.1 (*a*) Schematic drawing of the single-compartment model. Ca^{++} clearance from the cytosol includes extrusion via the plasma membrane, uptake into intracellular organelles, and binding to slow endogenous buffers. Two pools of endogenous rapid Ca^{++} buffers (*S*) and exogenously introduced buffers (*B*) are considered. (*b*) A single, brief calcium influx leads to an exponential $[Ca^{++}]_i$ transient (*left*). Changes in influx, buffering, or clearance parameters alter the shape of the transient (*middle* and *right*). For comparison, the control trace is drawn as dashed curves. (*c*) Summation of $[Ca^{++}]_i$ transients during a train of stimuli for 1 sec at 20 Hz (*left*). The accumulation of the average $[Ca^{++}]_i$ is described by an exponential rise to a steady-state plateau level *P* and an exponential decay. The dependence of the $[Ca^{++}]_i$ accumulation on changes in influx, buffering, and clearance is shown as in *b*. Note that a change in the Ca^{++}-binding ratio does not affect the plateau level.

homogeneous compartment. When is this assumption of spatial homogeneity justified? For a compartment of radius r, a characteristic diffusion time is given by $t_d = r^2/(6D_{Ca})$ where D_{Ca} is an effective Ca^{++}-diffusion constant that takes into account the slowdown of Ca^{++} diffusion caused by binding to cytosolic proteins (see Chapter 31). For $r = 1$ μm, which is the size of most mammalian nerve terminals and dendrites, and $D_{Ca} \approx 20\ \mu m^2\ sec^{-1}$ (Gabso et al. 1997), t_d is about 10 msec. Following the cessation of influx, Ca^{++} gradients dissipate within this time period. $[Ca^{++}]_i$ changes that occur on the time scale of 0.1 second (widely observed in small neural processes) can be well described using a single-compartment model that considers Ca^{++} influx, buffering, and clearance as the relevant biophysical processes (Figure 33.1a). The approximations used to describe these processes are discussed below.

- *Influx.* We limit our attention to pulses of calcium influx that are brief compared to the time required for calcium clearance. This condition is quite reasonable for short depolarizing voltage steps and, in particular, for the calcium influx through voltage-gated calcium channels during the repolarizing phase of an action potential that lasts less than a millisecond (Borst and Helmchen 1998). Ca^{++} clearance times in presynaptic terminals and dendrites are typically two orders of magnitude longer. A brief Ca^{++} pulse at time t_p can be described by a delta function and the increase in total calcium concentration ($\Delta[Ca^{++}]_T$),

$$j_{in} = \Delta[Ca^{++}]_T \delta(t - t_p) = \frac{Q_{Ca}}{2FV} \delta(t - t_p) \qquad (1)$$

where F is Faraday's constant, V the volume of the cellular compartment, and Q_{Ca} the calcium charge injected.

- *Buffering.* Most of the calcium ions entering the cytosol become bound by endogenous calcium-binding proteins and exogenous calcium buffers introduced into the cell by the experimenter (see Chapter 31). The initial changes in free-calcium concentration depend on the Ca^{++}-buffering capacity of the rapid Ca^{++} buffers. Usually, a pool *S* of rapid endogenous buffers and a pool *B* of exogenously introduced, rapid buffers are considered (Figure 33.1a). The Ca^{++}-binding ratio of the exogenous buffer (κ_B) is defined as the ratio of the change in buffer-bound Ca^{++} over the free Ca^{++} change (Neher and Augustine 1992). κ_B depends on the total buffer concentration $[B]_T$, its dissociation constant K_d, and $[Ca^{++}]_i$

$$\kappa_B = \frac{\partial[BCa]}{\partial[Ca^{++}]_i} = \frac{[B]_T K_d}{([Ca^{++}]_i + K_d)^2} \approx \frac{[B]_T}{K_d} \quad ([Ca^{++}]_i << K_d) \qquad (2)$$

An analogous expression exists for the Ca^{++}-binding ratio of the endogenous buffer (κ_S). The maximal Ca^{++}-binding ratio ($[B]_T/K_d$) occurs at $[Ca^{++}]_i$ levels that are well below the K_d. In its simplest version, the single-compartment model assumes that κ_S and κ_B are $[Ca^{++}]_i$-independent, corresponding to the idea that there are only small $[Ca^{++}]_i$ changes from a resting level during the experiment. Under these conditions, changes in free calcium concentration are proportional to changes in total calcium concentration (see Equation 5). A value of $\kappa_B = 100$ implies that for each free calcium ion, there are 100 ions bound to the buffer *B*. Note that Ca^{++}-binding ratios are dimensionless and that experimentally determined values for the endogenous buffers range from 50 to 2000 (Table 33.1). Also note that Ca^{++} indicators, which generally have fast kinetics, are potent, exogenous Ca^{++} buffers and therefore have to be included in pool *B*.

- *Clearance.* Calcium ions are either sequestered into intracellular organelles or extruded via the plasma membrane until $[Ca^{++}]_i$ decays back to a resting level of typically 50–100 nM. Most single-compartment models used for the analysis of experimental imaging data have used a calcium clearance mechanism that is linearly dependent on the deviation of $[Ca^{++}]_i$ from the resting calcium level with a clearance rate γ

$$j_{out} = -\gamma\Delta[Ca^{++}]_i = -\gamma([Ca^{++}]_i - [Ca^{++}]_{rest}) \quad (3)$$

This expression provides a good fit to experimental data in several systems (Neher and Augustine 1992; Tank et al. 1995; Helmchen et al. 1996, 1997). Nevertheless, Equation 3 is generally considered to be the low $[Ca^{++}]_i$ limit of a saturable, enzyme-driven extrusion mechanism; e.g., one following Michaelis-Menten kinetics. The good agreement with experimental data suggests that saturation effects might only be found under rather extreme stimulus conditions.

Dynamics of Single $[Ca^{++}]_i$ Transients

Combining the above kinetic descriptions for influx, buffering, and clearance, the differential equation for the temporal dynamics of $[Ca^{++}]_i$ following a single, brief calcium influx is

$$\frac{d[Ca^{++}]_T}{dt} = j_{in} + j_{out} \quad (4)$$

$$\frac{d[Ca^{++}]_i}{dt}(1 + \kappa_S + \kappa_B) = \Delta[Ca^{++}]_T\delta(t - t_p) - \gamma\Delta[Ca^{++}]_i$$

This equation simply states that the change in total calcium equals the increase in calcium minus the clearance. Assuming constant Ca^{++}-binding ratios, the analytical solution of Equation 4 is an exponential function with amplitude A and decay-time constant τ (Figure 33.1b). The relationships between A and τ and the model parameters are as follows:

$$A = \frac{Q_{Ca}/(2FV)}{(1 + \kappa_S + \kappa_B)} \quad (5)$$

$$\tau = \frac{(1 + \kappa_S + \kappa_B)}{\gamma} \quad (6)$$

Both A and τ depend on the Ca^{++}-binding ratios. However, the product $A\tau$, which is the integral of the $[Ca^{++}]_i$ transient (the area "underneath" the exponential curve), is independent of the Ca^{++}-binding ratios. Figure 33.1b illustrates that changes in influx, total buffering capacity, and clearance rate lead to specific changes of the $[Ca^{++}]_i$-transient shape (Sabatini and Regehr 1995). Although changes in influx or clearance only affect either A or τ, both magnitudes depend on the Ca^{++}-buffering capacity. Because of this dependence, A and τ may be altered by introducing a calcium indicator dye. A description of how this can be exploited to obtain an estimate of the endogenous Ca^{++}-binding ratio κ_S is given below.

Table 33.1. *Some representative experimental results for the basic parameters of calcium dynamics in dendrites and nerve terminals*

Preparation	Amplitude A (nM)	Time constant τ (msec)	Ca^{++}-binding ratio κ_S	Clearance rate γ (sec^{-1})	References
Dendrites					
Neocortical L5 pyramidal neurons	260	70	120	1700	Helmchen et al. (1996)
Hippocampal CA1 neurons	150	90	180	2000	Helmchen et al. (1996)
Cerebellar Purkinje cells	—	400	900–2000	—	Callewaert et al. (1996); Fierro and Llano (1996)
Neocortical L2/3 pyramidal neurons in vivo	—	100	—	—	Svoboda et al. (1997)
Nerve terminals					
Hippocampal mossy fiber terminals	5–10	1000	—	—	Regehr et al. (1994)
Crayfish neuromuscular junction	5–10	4000	600	80–100	Tank et al. (1995)
Cerebellar granule cell to Purkinje cell synapse	300	150	—	—	Regehr and Atluri (1995)
Frog retinotectal synapse	140	100	—	—	Feller et al. (1996)
Hippocampal CA3-CA1 synapse	—	40	—	—	Sinha et al. (1997)
Calciform terminals in brain stem	400–500	50	40	900	Helmchen et al. (1997)

The reported amplitudes and time constants refer to single action potential-evoked $[Ca^{++}]$ transients. They depend on the exogenous buffer conditions and temperature (see original publications for specific conditions). (–) Indicates not determined.

Summation of $[Ca^{++}]_i$ Transients during Repetitive Calcium Influx

If multiple calcium influx pulses occur on a time scale short compared to the $[Ca^{++}]_i$-decay time, the amplitude of the $[Ca^{++}]_i$ transient simply increases corresponding to the greater total calcium charge Q_{Ca}. For example, the amplitude of $[Ca^{++}]_i$ transients has been shown to scale approximately linearly with the number of high-frequency action potentials in presynaptic terminals (Regehr et al. 1994), in Purkinje cell axons (Callewaert et al. 1996), and in mammalian pyramidal cell dendrites in vivo (Svoboda et al. 1997). Such a linear increase would be expected to break down for more stimuli when calcium influx per pulse changes or saturation of buffers and pumps occurs. A linear sum of individual transients can also approximate the buildup of $[Ca^{++}]_i$ during repetitive calcium influx as it occurs during firing of a neuron at a lower constant frequency. We consider a train of stimuli starting at time $t = 0$ and with a time interval of Δt (frequency $f = 1/\Delta t$). The $[Ca^{++}]_i$ level above resting level immediately before the $(n+1)^{th}$ stimulus is given by a geometric progression (Regehr et al. 1994):

$$\Delta[Ca^{++}]_i(n\Delta t) = A\sum_{i=1}^{n} e^{-(i\Delta t)/\tau} = \frac{A}{(e^{\Delta t/\tau} - 1)}(1 - e^{-(n\Delta t)/\tau}) \qquad (7)$$

where A is the amplitude and τ the time constant of each individual transient. For stimulation frequencies $f < 1/(2\tau)$, there is little buildup and individually spaced transients result, but for higher frequencies, the transients add up; $[Ca^{++}]_i$ exponentially reaches a steady state in which influx and clearance balance, and $[Ca^{++}]_i$ fluctuates around a plateau level (Figure 33.1c). The time constant of the rise and the decay following the end of stimulation both are given by τ. The mean plateau level P reached at steady state is proportional to the frequency (Tank et al. 1995; Helmchen et al. 1996):

$$P = A\tau f = \frac{Q_{Ca}}{2FV\gamma} f \qquad (8)$$

with the integral of the single calcium transient ($A\tau$) as proportionality constant. P is independent of the Ca^{++}-binding ratios, indicating that Ca^{++} buffers can affect the transient dynamics of $[Ca^{++}]_i$ but not its steady-state levels. Figure 33.1c summarizes the effects of changes in influx, buffering, and clearance on the $[Ca^{++}]_i$ accumulation during repetitive stimulation. As in the case of the single $[Ca^{++}]_i$ transient, each change in these biophysical parameters leads to a characteristic alteration of the overall shape of the $[Ca^{++}]_i$ change (Tank et al. 1995).

APPLICATIONS OF THE SINGLE-COMPARTMENT MODEL

Changes in calcium dynamics similar to those illustrated in Figure 33.1b and c have been measured in small cell somata, presynaptic terminals, dendrites, and axons. The results of these experiments provide evidence for the applicability of the single-compartment model as well as quantitative estimates for the model parameters. Table 33.1 provides a comparison of observed parameters and lists the corresponding references.

Estimates of Endogenous Ca^{++}-binding Ratio and Clearance Rate

The endogenous Ca^{++}-binding ratio κ_S and the clearance rate γ can be estimated by measuring changes in the $[Ca^{++}]_i$ -transient decay time produced by increasing concentrations of an exogenous Ca^{++} buffer such as BAPTA or Fura-2 (Figure 33.2a). This follows directly from Equation 6, which can be rearranged to give:

$$\begin{aligned} \tau &= a_1\kappa_B + a_0 \\ a_1 &= 1/\gamma \\ a_0 &= (1 + \kappa_S)/\gamma \end{aligned} \qquad (9)$$

The decay time constant τ should be linearly related to the exogenous buffer capacity κ_B (Tank et al. 1991). The inverse of the measured slope (a_1) provides the clearance rate and the negative x-axis intercept ($-a_0/a_1$) provides an estimate of the endogenous

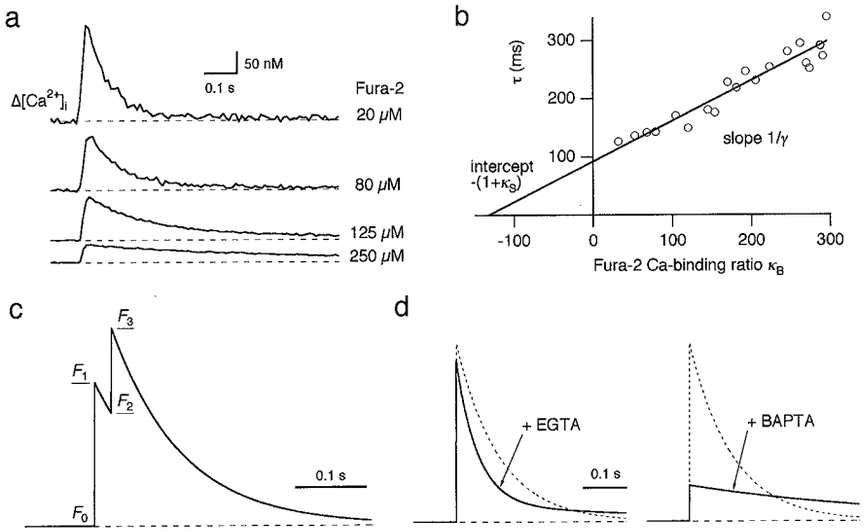

Figure 33.2. (*a*) Amplitude and decay time of calcium transients evoked by single action potentials in dendrites of neocortical pyramidal neurons depend on the Fura-2 concentration. (*b*) The endogenous Ca^{++}-binding ratio κ_S and the clearance rate γ can be quantified by measuring the dependence of the decay-time constant on the exogenously introduced Ca^{++} buffering capacity. (*c*) The amplitude A of the $[Ca^{++}]_i$ transient can be estimated from the degree of saturation of a fluorescent indicator with a known dissociation constant (see text). Schematic drawing of the indicator fluorescence change upon two brief calcium injections. The $[Ca^{++}]_i$ change per stimulus is assumed to be equal, but the change in fluorescence F is smaller for the second stimulus. (*d*) Schematic illustration of the effect of adding Ca^{++} buffers with different kinetic properties on individual control calcium transients (*dashed curves*). The fast buffer BAPTA changes the $[Ca^{++}]_i$ transient shape according to equilibrium considerations. A slow buffer like EGTA, in contrast, leads to a faster initial decay and a subsequent slow phase which are explained by its slow association rate. (*a, b* reprinted, with permission, from Helmchen et al. 1996.)

buffer capacity κ_B (Neher and Augustine 1992). An example of this method, taken from a study of $[Ca^{++}]_i$ transients in pyramidal cell dendrites, is shown in Figure 33.2b. Two methods have been employed to provide known exogenous buffer concentrations: dialysis with patch pipets (Neher and Augustine 1992; Helmchen et al. 1996, 1997) and intracellular sharp-microelectrode injection of a fluorescent buffer from which estimated concentrations can be calculated from the fluorescence intensity (Tank et al. 1995).

Estimates of Amplitude A and Total Calcium Charge Q_{Ca}

Compared to the unaltered $[Ca^{++}]_i$ transients, the amplitude A which is obtained from a Ca^{++} indicator measurement is reduced by a factor $(1 + \kappa_S)/(1 + \kappa_S + \kappa_B)$ (see Equation 5). A can either be measured ratiometrically or estimated from the degree of saturation of the fluorescent dye (see below). If the total buffering capacity of the cytoplasm is known and with an estimate of the compartment volume from morphology, the total calcium charge Q_{Ca} can be calculated by rearranging Equation 5:

$$Q_{Ca} = 2FVA(1 + \kappa_S + \kappa_B) \tag{10}$$

Alternatively, Q_{Ca} can be measured directly using excessive dye loading of the compartment to obtain fluorescence changes proportional to Q_{Ca} (Neher 1995; Borst and Helmchen 1998; see Chapter 32). If individual calcium transients cannot be easily resolved, Q_{Ca} can be determined from the frequency dependence of the initial slope of the calcium buildup produced by a train of action potentials (Tank et al. 1995).

DEVIATIONS FROM LINEAR BEHAVIOR

If $[Ca^{++}]_i$ changes are appreciable compared to the dissociation constant of the dominant intracellular buffers, or when buffer kinetics are slow compared to the decay time constant, exponential decaying transients are not observed. Here we describe expected deviations under these two circumstances.

Saturation of Buffers and Pumps

If buffer kinetics are still rapid but $[Ca^{++}]_i$ changes become appreciable compared to the K_d values of the intracellular buffers, then Equation 4 is still appropriate, but κ_B and κ_S are not constant and the solution is not an exponential decay. Numerically calculated decay curves as well as measured transients show pronounced upward curvature (faster decays) at higher $[Ca^{++}]_i$ levels on a semi-log plot (Tank et al. 1995) because the effective buffering capacity is reduced at these levels due to partial saturation of the buffers. An opposite effect would be expected from saturation of clearance mechanisms at very high $[Ca^{++}]_i$ levels. Saturation in the clearance rate would be

expected to also alter the linear frequency dependence of the plateau level during long stimulus trains (Equation 8). A related buffer saturation effect can be exploited to advantage to provide an estimate of the amplitude A of individual $[Ca^{++}]_i$ transient when ratiometric measurements of absolute calcium concentration are not feasible, for example when fluorescence is measured from a large region of AM-loaded brain slices or intact brains (Regehr and Atluri 1995; Feller et al. 1996). Except when confocal or two-photon techniques for volume resolution are used, such measurements contain contaminating fluorescence from other structures. In these cases, A can be estimated from the degree of saturation of a high-affinity calcium indicator (Regehr and Atluri 1995; Sabatini and Regehr 1995; Feller et al. 1996). Figure 33.2c shows the fluorescence change of an indicator evoked by two subsequent brief calcium injections. The second injection evokes a smaller fluorescence change than the first one due to partial saturation of the indicator. Assuming that the change in calcium concentration is the same for the two stimuli, its magnitude can be estimated from the ratio α of the two fluorescence changes:

$$\Delta[Ca^{++}]_i = \frac{([Ca^{++}]_{rest} + K_d)(1 - \alpha)}{2\alpha} \tag{11}$$

where $\alpha = (F_3 - F_2)/(F_1 - F_0)$ and assuming $F_2 \approx F_1$ (Feller et al. 1996). This method, however, relies on reasonable estimates of the resting $[Ca^{++}]_i$ level and the dissociation constant of the indicator.

Slow Buffers

Radical departures in calcium dynamics from the expected results (Equations 4–6) have been observed when slow calcium buffers such as EDTA or EGTA are introduced as exogenous buffers into presynaptic nerve terminals (Atluri and Regehr 1996; Feller et al. 1996) and nerve-cell dendrites (Markram et al. 1998). A comparison between the effects on a $[Ca^{++}]_i$ transient of adding a fast buffer, BAPTA, versus a slow buffer, EGTA, is illustrated schematically in Figure 33.2d. Addition of BAPTA reduces the amplitude of the transient while prolonging its decay, consistent with what is expected from Equations 5 and 6. Addition of EGTA, however, has only a slight effect on the amplitude A but changes the shape of the transient by providing a faster initial decay while also producing a slower subsequent phase. As easily demonstrated in numerical simulations, the early faster decay is produced by Ca^{++} binding to EGTA on a time scale longer than the response time of the Ca^{++} indicator (Atluri and Regehr 1996; Feller et al. 1996; Markram et al. 1998). The fast-time constant can be approximated by adding the association rate of Ca^{++} binding of EGTA to the clearance mechanisms (Atluri and Regehr 1996):

$$\tau_{fast} = \frac{(1 + \kappa_S + \kappa_B)}{\gamma + k^{on}_{EGTA}[EGTA]} \tag{12}$$

The longer time constant of the second decay phase is produced by the same mechanism as for BAPTA: More bound calcium must be removed per unit change of free calcium ion concentration change. This time constant is given by Equation 6 after addition of the Ca^{++}-binding ratio κ_{EGTA}.

SINGLE-COMPARTMENT MODELS AND THE MEASUREMENT OF CALCIUM-DRIVEN REACTIONS

The single-compartment models we have summarized here were developed to explain basic properties of calcium transients observed in imaging experiments on small structures such as presynaptic terminals and dendrites. The analysis also provides a set of tools to alter calcium dynamics, however, which has proven to be important in biophysical characterization of calcium-driven reactions. For example, the systematic prolongation of calcium transients with increasing exogenous buffer concentrations helped to demonstrate that the time constant of $[Ca^{++}]_i$ decay was the rate-limiting step in the decay of calcium-driven short-term synaptic enhancement at an invertebrate synapse (Delaney and Tank 1994). In a mammalian synapse, exogenous buffer addition and calcium plateau manipulation by changes in stimulus frequency were used to alter calcium dynamics, in order to determine kinetic rate constants of a calcium-driven reaction involved in short-term synaptic enhancement (Regehr et al. 1994). Similar approaches have been used in the characterization of vesicle mobilization in chromaffin cells (Heinemann et al. 1993), mitochondrial Ca^{++} uptake and release in bullfrog sympathetic neurons (Friel and Tsien 1994), adaptation of cellular excitability (Sobel and Tank 1994), and synaptic facilitation in the cerebellum (Atluri and Regehr 1996).

CONCLUSION

In summary, we have described the basic equations and parameters of a simple model of calcium dynamics that is applicable to action-potential-evoked $[Ca^{++}]_i$ transients in nerve terminals and dendrites. Methods have been introduced to quantify the main parameters of calcium influx, buffering, and clearance. The single-compartment model is well suited as a starting point for a more detailed characterization of Ca^{++} handling in small cellular compartments.

REFERENCES

Atluri P.P. and Regehr W.G. 1996. Determinants of the time course of facilitation at the granule cell to Purkinje cell synapse. *J. Neurosci.* **16:** 5661–5671.

Borst J.G. and Helmchen F. 1998. Calcium influx during an action potential. *Methods Enzymol.* **293:** 352–371.

Callewaert G., Eilers J., and Konnerth A. 1996. Axonal calcium entry during fast "sodium" action potentials in rat cerebellar Purkinje neurones. *J. Physiol.* **495:** 641–647.

Delaney K.R. and Tank D.W. 1994. A quantitative measurement of the dependence of short-term synaptic enhancement on presynaptic residual calcium. *J. Neurosci.* **14:** 5885–5902.

Feller M.B., Delaney K.R., and Tank D.W. 1996. Presynaptic calcium dynamics at the frog retinotectal synapse. *J. Neurophysiol.* **76:** 381–400.

Fierro L. and Llano I. 1996. High endogenous calcium buffering in Purkinje cells from rat cerebellar slices. *J. Physiol.* **496:** 617–625.

Friel D.D. and Tsien R.W. 1994. An FCCP-sensitive Ca^{2+} store in bullfrog sympathetic neurons and its participation in stimulus-evoked changes in $[Ca^{2+}]_i$. *J. Neurosci.* **14:** 4007–4024.

Gabso M., Neher E., and Spira M.E. 1997. Low mobility of the Ca^{2+} buffers in axons of cultured Aplysia neurons. *Neuron* **18:** 473–481.

Heinemann C., von Rüden L., Chow R.H., and Neher E. 1993. A two-step model of secretion control in neuroendocrine cells. *Pflueg. Arch. Eur. J. Physiol.* **424:** 105–112.

Helmchen F., Borst J.G.G., and Sakmann B. 1997. Calcium dynamics associated with a single action potential in a CNS presynaptic terminal. *Biophys. J.* **72:** 1458–1471.

Helmchen F., Imoto K., and Sakmann B. 1996. Ca^{2+} buffering and action potential-evoked Ca^{2+} signaling in dendrites of pyramidal neurons. *Biophys. J.* **70:** 1069–1081.

Markram H., Roth A., and Helmchen F. 1998. Competitive calcium binding: Implications for dendritic calcium signaling. *J. Comput. Neurosci.* **5:** 331–348.

Neher E. 1995. The use of fura-2 to estimate Ca buffers and Ca fluxes. *Neuropharmacology* **34:** 1423–1442.

Neher E. and Augustine G. 1992. Calcium gradients and buffers in bovine chromaffin cells. *J. Physiol.* **450:** 273–301.

Regehr W.G. and Atluri P.P. 1995. Calcium transients in cerebellar granule cell presynaptic terminals. *Biophys. J.* **68:** 2156–2170.

Regehr W.G. and Tank D.W. 1994. Dendritic calcium dynamics. *Curr. Opin. Neurobiol.* **4:** 373–382.

Regehr W.G., Delaney K.R., and Tank D.W. 1994. The role of presynaptic calcium in short-term enhancement at the hippocampal mossy fiber synapse. *J. Neurosci.* **14:** 523–537.

Sabatini B.L. and Regehr W.G. 1995. Detecting changes in calcium influx which contribute to synaptic modulation in mammalian brain slice. *Neuropharmacology* **34:** 1453–1467.

Sinha S.R., Wu L.-G., and Saggau P. 1997. Presynaptic calcium dynamics and transmitter release evoked by single action potentials at mammalian synapses. *Biophys. J.* **72:** 637–651.

Sobel E.C. and Tank D.W. 1994. In vivo Ca^{2+} dynamics in a cricket auditory neuron: An example of chemical computation. *Science* **263:** 823–826.

Svoboda K., Denk W., Kleinfeld D., and Tank D.W. 1997. *In vivo* dendritic calcium dynamics in neocortical pyramidal neurons. *Nature* **385:** 161–165.

Tank D.W., Regehr W.G., and Delaney K.R. 1991. Modeling a synaptic chemical computation: The buildup and decay of presynaptic calcium. *Soc. Neurosci. Abstr.* **17:** 578.

———. 1995. A quantitative analysis of presynaptic calcium dynamics that contribute to short-term enhancement. *J. Neurosci.* **15:** 7940–7952.